# Sun glint correction of very high spatial resolution images

***G. Doxani, M. Papadopoulou, P. Lafazani, M. Tsakiri - Strati, E. Mavridou***

*Department of Cadastre, Photogrammetry and Cartography,*
*Aristotle University of Thessaloniki, Thessaloniki, Greece*

**Abstract:** Sun glint is often evident in remotely sensed imagery data of very high spatial resolution that depict aquatic environment. The problem occurs when the water surface is not flat and the sun radiation is directly reflected to the sensor affecting the pixel brightness values. The state of water surface, sun position and viewing angle are the main function parameters to estimate glint effect on the images. The removal of glint is compulsory since multispectral bathymetry and bottom types mapping are affected unfavourably. In this paper two widely applied methodologies were investigated towards correcting from sun glint effect optical satellite images of very high spatial resolution. Particularly, the approaches proposed by Lyzenga (1985) and Hedley et al. (2005) were applied on images acquired by Ikonos-2 and Worldview-2. The experimental results indicated the effectiveness of both methods in correcting glint contaminated imagery datasets.

## 1. Introduction

Remotely sensed imagery data have been considered as a cost- and time-effective solution to accurate surveys over water areas during the last years, i.e. bathymetric measurements (Lyzenga, 1985; Stumpf et al., 2003; Goodman et al., 2008; Su et al., 2008) and benthic habitat mapping (Capolsini et al., 2003; Hochberg et al., 2003). The implementation and the accuracy of these image processes are often impeded by the appearance of glint on the images. The combination of atmospheric and water surface conditions with the solar and view angle during image acquisition is responsible for sun glint effect (Goodman et al., 2008; Lyzenga, 2006; Hochberg et al., 2003). Hedley et al. (2005) defined glint as the specular reflection of sunlight from aquatic area into the sensor filed of view.

Kay et al. (2009) proposed that a direct and efficient way to avoid glint is by selecting the proper time and place of image acquisition. Many satellite instruments (i.e. SeaWiFS, OCTS and CZCS) can tilt 20$^{o}$ from nadir to minimize sun glint. However there are instruments that do not have the tilting capability and so the glint avoidance is not possible. This also stands for high resolution sensors that are primarily used for land observation and the avoidance of sea areas glint is neglected.

Thus, a variety of methodologies have been developed and implemented to date

towards correcting glint from remotely sensed data, i.e. hybrid airborne sensor data (Lyzenga, 1985), satellite images of high resolution (Hochberg et al., 2003; Hedley et al., 2005) and hyperspectral imagery data (Goodman et al., 2008). Kay et al. (2009) provided a thorough review of current glint correction techniques. The available methods can be grouped in two main categories depending on the area of application, i.e. open ocean and shallow waters. The imagery data for open ocean applications have spatial resolution on the scale of 100–1000 m. The glint estimation in this case is based on the wind speed and direction that affect the sea surface slope and cause glint (Cox and Munk, 1954; Wang and Bailey, 2001). The implementations outcomes are constrained by glint contamination with the greatest errors to be in image areas with the brightest glint pixels. Methods of second category employ imagery data of high spatial resolution (<10m) acquired over shallow coastal environments. The main assumption in this case is that the water leaving radiance in the near-infrared (NIR) should approach zero; hence, any NIR signal remaining after atmospheric correction must be due to sun glint. The estimated glint value and the pixel values of visible bands are then used to form the function for glint correction.

The aim of this paper was to evaluate the two widely applied methodologies proposed by Lyzenga (1985) and Hedley et al. (2005) towards correcting sun glint from imagery data with high spectral and spatial resolution. In particular the multiplicity of the Worldview-2 bands was investigated concerning the optimum band combination for sun glint removal. The processing outcomes were compared with the corresponding results of an Ikonos-2 image (Mavridou, 2012) that depicted the same study area.

## 2. Sun glint correction algorithms for high resolution images

There are several methods for glint removal from high resolution satellite images (Lyzenga, 1985; Hedley et al. 2005, Goodman et al. 2008; Kutser et al., 2009). In this paper, the widely applied algorithms of Lyzenga and the Hedley et al. are described and implemented. Both selected algorithms are applied through carefully selected samples of image pixels. The effectiveness of the methods relies on the appropriate choice of the pixel samples from an image region that is relatively dark, reasonably deep and with evident glint (Hedley et al., 2005; Edwards, 2010a).

### 2.1 The Lyzenga algorithm

The analysis of glint correction from multispectral images depicting swallow waters was introduced by Lyzenga (1985). According to his approach, sun glint is estimated by employing the covariance of visible band that was used for depth processing and near-infrared band. Considering that the high absorption of water at NIR band radiation should result to pixel brightness value close to zero, higher pixel values should imply atmospheric haze or glint effect.

The function for glint estimation $dR_{VIS}$, ignoring the atmospheric effect, is:

$$dR_{VIS} = \frac{\sigma_{VIS,NIR}}{\sigma^2_{NIR}}(R_{NIR} - Mean_{NIR}) \quad (1)$$

where VIS= visible band, NIR= infrared band, $\sigma_{VIS,NIR}$ is the covariance coefficient of visible and infrared band, $\sigma^2_{NIR}$ is the variance coefficient of infrared band, $R_{NIR}$ is the pixel value in NIR band and $Mean_{NIR}$ is the average of a deep-water sample of pixels in NIR band. The corrected pixel value $R'_{VIS}$ is then calculated by subtracting the 'glint quantity' (Eq.1) from the visible glinted band $R_{VIS}$:

$$R'_{VIS} = R_{VIS} - dR_{VIS} \quad (2)$$

Combining equations (1) and (2) the corrected pixel value can be written

$$R'_{VIS} = R_{VIS} - r(R_{NIR} - Mean_{NIR}) \quad (3)$$

where r is the ratio $\frac{\sigma_{VIS,NIR}}{\sigma^2_{NIR}}$

The proposed procedure demonstrated efficient results in case of images with a significant evidence of glint (Lyzenga, 1985). The Equation (3) can be also utilized for the correction of other atmospheric effects by estimating the corresponding variation coefficients (Eq.1). Nevertheless, the correction outcome is uncertain and inaccurate when both glint and other atmospheric effects are apparent on an image (Lyzenga, 2006).

## 2.2 The Hedley et al. algorithm

Hochberg et al. (2003) proposed a simple and innovative method employing a physical atmospheric model for glint removal in swallow waters. The initial consideration was the same with the one of Lyzenga (1985) that the radiance is highly absorbed by water at NIR band and so the pixel brightness value should tend to zero. This condition is not fulfilled due to glint appearance; in these cases the pixel values of NIR band determines the spatial variation of glint $f_g(x,y)$ for the pixel at $(x,y)$ spatial position. The $f_g(x,y)$ assessment is realized by scaling NIR band to the range zero to one. Zero corresponds to minimum pixel value (darkest pixel) and one to maximum pixel value (brightest pixel). The second consideration is that the refractive index is independent of wavelength; hence the brightness value of glint pixels $f_g(x,y)$ is equal for visible and infrared bands. The deglinted visible bands were resulted by subtracting the quantity $f_g(x,y)$ from the glinted pixel values.

Refining the approach of Hochberg et al. (2003), Hedley et al. (2005) introduced a

more simplified and robust methodology. The new suggestion was the use of one or more samples of image pixels rather than only two pixels, i.e. the brightest and the darkest one. The image processing for glint correction involves a linear regression analysis between the sample pixels of every visible band (y-axis) and the corresponding pixels of NIR band (x-axis) (Figure 1).

The image pixels are corrected according to the following equation:

$$R_i^{'} = R_i - b_i(R_{NIR} - Min_{NIR}) \quad (4)$$

where $R_i^{'}$ = the corrected pixel value, $R_i$ = the initial pixel value, $b_i$ = the regression line slope, $R_{NIR}$ = the corresponding pixel value in NIR band and $Min_{NIR}$ = the minimum NIR value existing in the sample. In Equation (3), the relative pixel values are employed; hence the estimation of the radiance values (absolute) is not required.

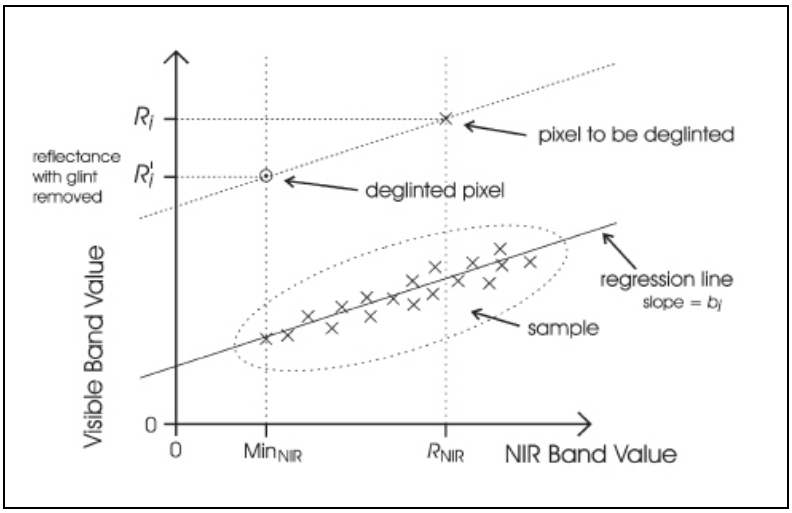


**Figure 1.** The regression analysis diagram between a visible and NIR brightness values. The pixels with no glint are homogeneous and close to the regression line. According to Hedley et al. (2005), the other pixels are corrected by estimating the slope of the regression and the minimum NIR brightness value of a sample.

This method is usually applied after atmospheric correction, but if the atmospheric conditions are considered uniform all over the study area it can be used at first.

From the comparison of Equation (3) and Equation (4) it is apparent that the two methods are similar. Their difference is that Lyzenga uses the mean value of NIR band while Hedley et al. use the minimum value (Kay et. al, 2009).

## 3. Imagery data and Study area

The efficiency of the glint correction algorithms were examined utilizing imagery

data of high spatial and spectral resolution. In particular the one dataset included the eight (8) bands of Worldview-2 multispectral image with spatial resolution of 2 m and acquisition date the 16th of June 2010. In addition the four (4) bands of Ikonos-2 multispectral image with spatial resolution of 1m and acquisition date the 1st of September 2007 involved in this study. The available data were geo-referenced to UTM (zone 34) system and WGS84.

The images depicted the coastal area of Nea Michaniona, Thessaloniki, in the northern part of Greece. There is a smooth variance of water depth in the study area and the water is clear. The shallower parts are covered with dense sea grass while the deeper ones are sandy. Despite the water clarity, the sun glint was sparsely evident in a great part of image scenes affecting the image quality and constraining the implementation of bathymetry applications (e.g. Doxani et al., 2012) as well as applications of bottom types mapping. The study area is presented in Figure 2 as it is depicted by Worldview-2 satellite.

From now on, the 8 bands of the Worldview-2 image will be symbolized as: band 1 (coastal), 2 (blue), 3 (green), 4 (yellow), 5 (red), 6 (red-edge), NR1 (first near-infrared) and NIR2 (second near-infrared) as well as the 4 bands of the Ikonos-2 image will be symbolized as: band 1 (blue), 2 (green), 3 (red), and 4 (near-infrared)

**Figure 2.** The Worldview-2 image of the study area (R:4,G:3,B:2). The glint effect is evident over the water area.

## 4. Glint correction process and results assessment

For the implementation of the proposed methodologies by Lyzenga (1985) and Hedley et al. (2005) three image samples with size 50x50 pixels were carefully

selected from glinted areas at different locations on the images of each dataset, i.e. Ikonos-2 and Worldview-2.

The two methodologies as described in §2 are proper for the study area since the water is clear, not very shallow (depth >=3 m) and vegetation in sea grass area does not reach the water surface. Both of them were applied before the atmospheric correction of the images.

The critical at this step of the procedure concerning the Worldview-2 image was the definition of the optimum band combination of NIR (two bands) and visible (six bands) bands that would be involved in the calculation. For this reason the relationship between each visible band with both NIR bands was examined trough scatter plots of visible bands versus NIR1 or NIR2 (Fig. 3). These graphs demonstrated that there was a significant linear relationship among the 'new' bands, i.e. band 1, band 4 and band 6 with the NIR2, and among the 'traditional' bands, band 2, band 3 and band 5 with the NIR1. This actually happens because the two groups of bands come from two separate sensors. Therefore the glint removal process was twofold in this case, one for each set of Worldview-2 bands. This grouping stood for the implementation of both glint correction methods.

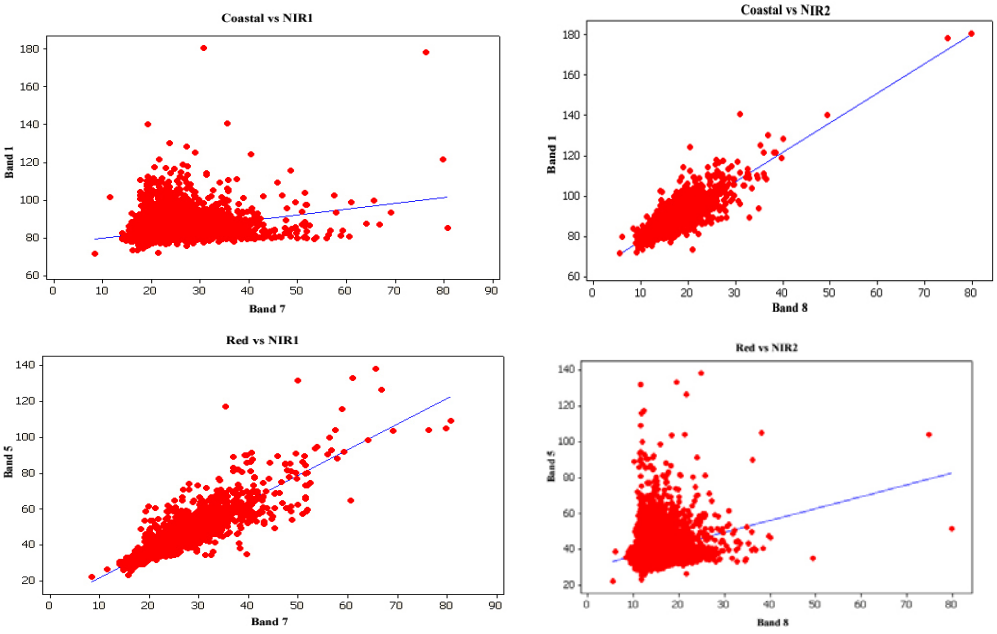


Figure 3. Scatter plots between visible bands and NIRs. Suggestively the linear relationship between the 'new' Band 1 vs NIR2, and the 'traditional' Band 5 vs NIR1 are depicted. The blue lines depict the models best fitted to the data.

The required statistics parameters to implement Lyzenga's (1985) sun glint correction methodology (Equation 2) are presented in Table 1. The resulted images are depicted in Figures 4 and 5.

**Table 1.** The parameters values used for the Lyzenga method implementation

| | Ikonos-2 | | | Worldview-2 | | | | | |
|---|---|---|---|---|---|---|---|---|---|
| | Band 4 | | | Band 7 | | | Band 8 | | |
| $\mathbf{Mean}_{NIR}$ | 5.495 | | | 22.634 | | | 14.072 | | |
| $\sigma^2_{NIR}$ | 1.25 | | | 4.659 | | | 2.024 | | |
| | **Band 1** | **Band 2** | **Band 3** | **Band 2** | **Band 3** | **Band 5** | **Band 1** | **Band 4** | **Band 6** |
| $\sigma_{VIS,NIR}$ | 1.148 | 1.322 | 1.467 | 6.553 | 7.849 | 6.468 | 2.947 | 4.956 | 3.447 |

In order to implement the methodology of Hedley et al. (2005) on the 'glint' image bands the regression slope was defined for every band combination and the Equation (4) was used to determine the corrected pixel values. The estimated parameters of linear regressions between the visible bands and the corresponding NIR band are presented in Table 2. As seen in Table 2, the values of the determination coefficients $\mathbf{R^2}$ (Lafazani, 2004) are statistically significant and indicate a correct calculation of slope $b_i$ (§2.2). The resulted images are presented in Figures 4 and 5.

**Table 2.** The results of the linear regressions between the visible bands and the corresponding NIR band in each case study. The slopes $b_i$ of regression lines and the corresponding coefficients of determination $\mathbf{R^2}$ are given.

| | Ikonos-2 | | | Worldview-2 | | | | | |
|---|---|---|---|---|---|---|---|---|---|
| | Band 4 | | | Band 7 | | | Band 8 | | |
| | **Band 1** | **Band 2** | **Band 3** | **Band 2** | **Band 3** | **Band 5** | **Band 1** | **Band 4** | **Band 6** |
| **Slope $b_i$** | 0.687 | 0.983 | 0.81 | 1.16 | 1.34 | 1.40 | 1.46 | 2.07 | 1.32 |
| $\mathbf{R^2}$ | 0.83 | 0.92 | 0.93 | 0.75 | 0.82 | 0.90 | 0.80 | 0.76 | 0.64 |

A certain way to evaluate the results of a glint correction methodology is to track the performance of the corrected images in a bathymetry application or a bottom type classification of the corrected area. Acceptable results in these two cases imply satisfactory removal of glint. A more simple and conventional way to assess the glint removal relies on optical observation of the corrected images as well as on profiles of the visible bands along lines carefully selected on proper areas of the image (Fig. 4ai, 5ai). Finally, the tracking of spectral profiles of pixels with glint and pixels without glint is indicative of a sufficient glint removal (Fig. 6).

The corrected bands of the Worldview-2 image as resulted after the implementation of sun glint correction methodologies are presented in Figure 4. Both outcomes were sufficiently improved even in the cases of very bright pixels, i.e. great glint contamination, as it can be seen on the visual representations (Fig. 4bi, Fig. 4ci) which are optically similar. For a more detailed assessment of the methods' results, the profiles of the bands of the original and the corrected images along the line depicted in red in Fig. 4, were constructed. The corrected profiles are smoother

and show that sufficient amount of glint has been removed. Furthermore, the Hedley et al. algorithm seems to keep the original relations among bands (Fig. 4cii) while the Lyzenga method causes concurrence of band 1 and band 2 (Fig. 4bii).

(a) Worldview-2 image with glint

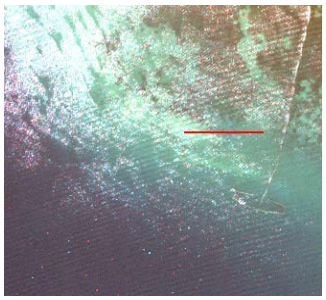

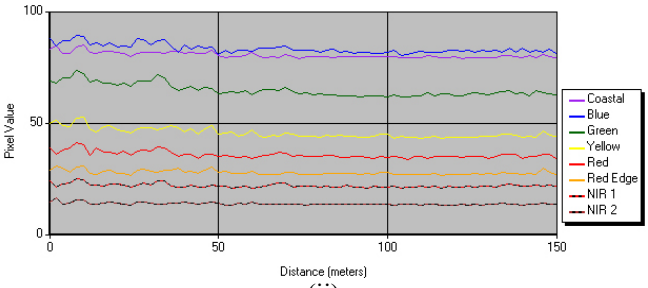


(i) (ii)

(b) Corrected image by Lyzenga (1985)

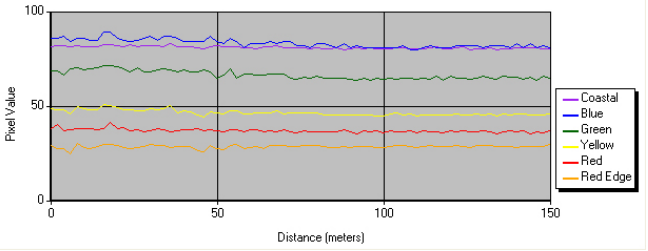


(i) (ii)

(c) Corrected image by Hedley et al. (2005)

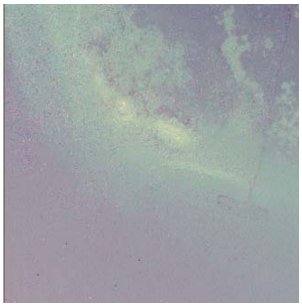

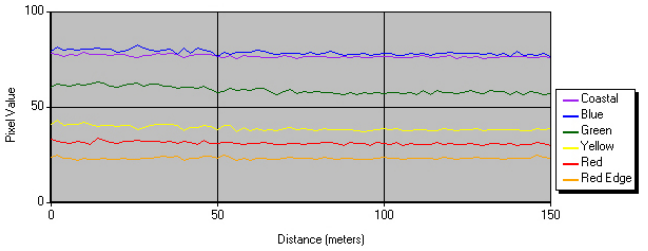


(i) (ii)

**Figure 4.** The implementation outcomes of the glint correction methodologies. The images are presented in column (i): (a) the Worldview-2 image with the glint effect to be apparent over the water area, the corrected images by the methods of (b) Lyzenga (1985) and (c) Hedley et al. (2005). In column (ii): the spatial profile of the red line in (a)(i) indicates the values of pixels with and without glint of (a) the Worldview-2 image bands and (b),(c) the corrected image bands.

(a) Ikonos-2 image with glint

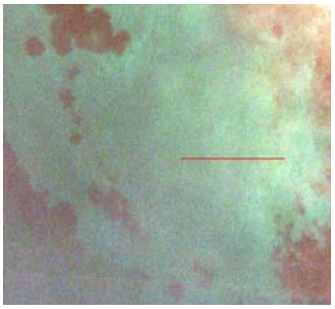

(i)

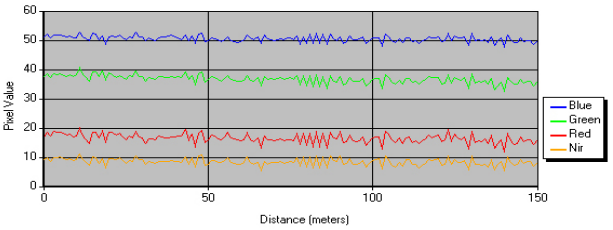


(ii)

(b) Corrected image by Lyzenga (1985)

(i)

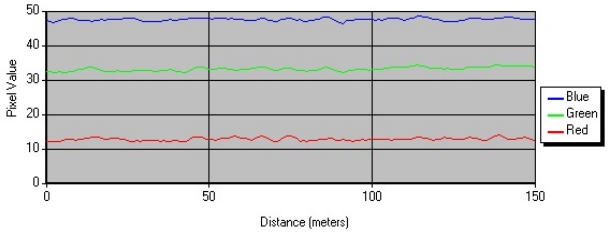


(ii)

(c) Corrected image by Hedley et al. (2005)

(i)

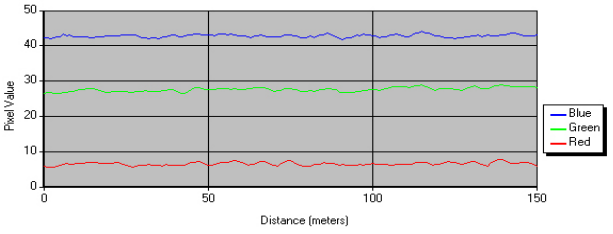


(ii)

**Figure 5.** The implementation outcomes of the glint correction methodologies. The images are presented in column (i): (a) the Ikonos-2 image with the glint effect to be apparent over the water area, the corrected images by the methods of (b) Lyzenga (1985) and (c) Hedley et al. (2005). In column (ii): the spatial profile of the red line in (a)(i) indicates the values of pixels with and without glint of (a) the Worldview-2 image bands and (b),(c) the corrected image bands.

The corrected bands of the Ikonos-2 image as resulted after the implementation of sun glint correction methodologies are presented in Figure 5. For this image also, the outcomes were sufficiently improved even in the cases of very bright pixels. Furthermore, the resulted images (Fig. 5bi, 5ci) are optically similar. Again for a detailed assessment of the glint removal the profiles of the original and corrected bands were constructed. The corrected profiles are much smoother than the originals and show that significant amount of glint has been removed. In case of Ikonos-2, both algorithms seem to keep the relations among bands (Fig. 5bii, 5cii) after the glint correction.

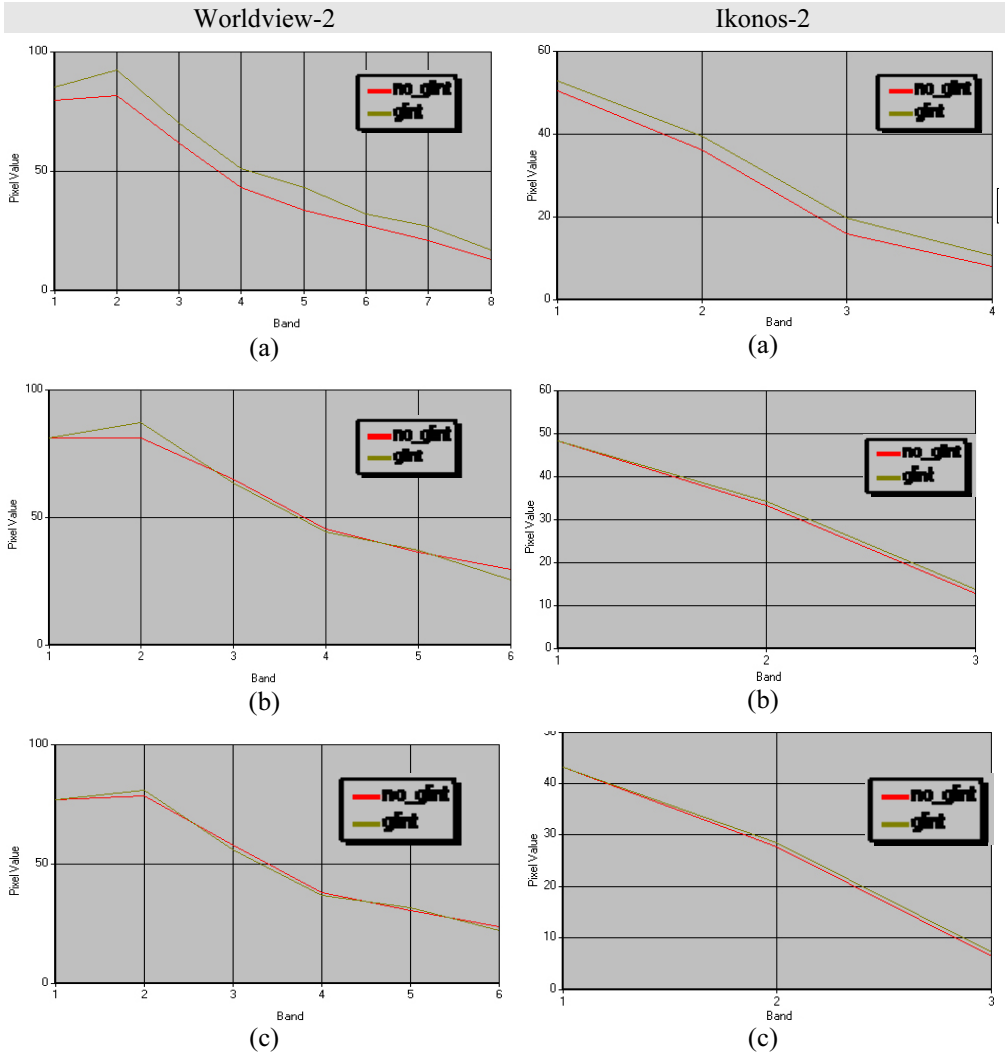


**Figure 6.** The spectral profile of a pixel with glint (green line) and a pixel with no glint (red line) in the: a) initial images with glint, b) corrected images by Lyzenga (1985) and c) corrected images by Hedley et al. (2005).

Along with the previous, the spectral profiles of a pixel with glint and of a pixel without glint were constructed for each image set (original and corrected bands) (Fig. 6). According to these profiles the Lyzenga algorithm yield a better result for the Ikonos-2 set since the spectral profile of the corrected pixel was almost identical with the one with no glint. On the other hand the Hedley et al. algorithm produced good results for both Ikonos-2 and Worldview-2 images. In this case the profiles of contaminated and corrected pixels are almost identical in both sets.

## 5. Conclusions

In this paper, two widely applied algorithms for sun glint correction were tested on two high resolution multispectral image sets i.e. Ikonos-2 and Worldview-2. According to the theoretical description (§2.1, 2.2) the two algorithms are based on similar hypothesis, something that is also verified through the optical observation of the corrected images and the illustration of the profiles behavior.

According to the form of the profiles, the Ikonos-2 set responses better to the application of both methodologies. On the other hand in the case of Worldview-2, the Lyzenga methodology causes concurrence of band 1 and band 2. This could affect the depth calculation or the benthos observation unfavorably. In general the outcomes of the above investigation indicated that the Hedley et. al. approach produced improved results on both high resolution multispectral sets.

## References


Capolsini, P., Andréfouët, S., Rion, C. and Payri, C., 2003. *A comparison of Landsat ETM+, SPOT HRV, IKONOS, ASTER and airborne MASTER data for coral reef habitat mapping in South Pacific islands*. Canadian Journal of Remote Sensing, 29, pp. 187–200

Cox, C. and Munk, W., 1954. *Statistics of the Sea Surface Derived from Sun Glitter*. J. Mar. Res. 1954, 13, 198-227.

Doxani, G., Lafazani P., Papadopoulou M., Tsakiri-Strati M. and Pikridas C., 2012. *Shallow-water bathymetry over variable bottom types using multispectral Worldview-2 image*. The XXII Congress of the International Society of Photogrammetry and Remote Sensing, 25 Aug-1 Sept, Melbourne, Australia

Edwards A.J., 2010a. *Les. 5: Removing sun glint from compact airborn spectrographic imager (CASI) imagery*. Bilko module 7, UNESCO. http://www.noc.soton.ac.uk/bilko/module7/m7_15.php (8 Jan. 2012)

Goodman, J.A., Lee, Z. and Ustin, S.L., 2008. *Influence of Atmospheric and Sea-Surface Corrections on Retrieval of Bottom Depth and Reflectance Using a Semi-Analytical Model: A Case Study in Kaneohe Bay, Hawaii*. Appl. Opt., 47, F1-F11.

Hedley, J.D., Harborne A.R. and Mumby, P.J., 2005. *Simple and robust removal of sun glint for mapping shallow-water benthos*. Int. Journal of Remote Sensing, 26(10) pp. 2107-2112.

Hochberg, E.J., Andrefouet S. and Tyler, M.R., 2003. *Sea surface correction of high spatial resolution Ikonos images to improve bottom mapping in near-shore environments*. IEEE Transactions on Geoscience and Remote Sensing, 41(7), pp. 1724-1729.

Kay S., Hedley J.D. and Lavender S, 2009. *Sun Glint Correction of High and Low Spatial Resolution Images of Aquatic Scenes: a Review of Methods for Visible and Near-Infrared Wavelengths*. Remote Sens. 1, pp. 697-730.

Kutser, T. Vahtmäe, E. and Praks, J.A., 2009. *Sun Glint Correction Method for Hyperspectral Imagery Containing Areas with Non-Negligible Water Leaving NIR Signal*. Remote Sens. Environ. 2009, 113, pp. 2267-2274.

Lafazani P., 2004. *Methods of Geographical Analysis*. Lecture notes, Department of Cadastre, Photogrammetry and Cartography, AUTH (in greek)

Lyzenga, D., 1985. *Shallow-water bathymetry using combined lidar and passive multispectral scanner data*. Int. Journal of Remote Sensing, 6(1), pp. 115-125.

Lyzenga, D., Malinas N. and Tanis, F., 2006. *Multispectral bathymetry using a simple physically based algorithm*. IEEE Transactions on Geoscience and Remote Sensing, 44(8), pp. 2251-2259.

Mavridou E.R., 2012. *Creation of digital bathymetric maps using multispectral bathymetry*. MSc Thesis, Department of Cadastre, Photogrammetry and Cartography, AUTH (in greek)

Stumpf, R., Holderied K. and Sinclair, M., 2003. *Determination of water depth with high-resolution satellite imagery over variable bottom types*. Limnol. Oceanogr., 48(1, part 2), pp. 547-556.

Su, H., Liu H. and Heyman, W., 2008. *Automated derivation for bathymetric information for multispectral satellite imagery using a non-linear inversion model*. Marine Geodesy, 31, pp. 281-298.

Wang, M. and Bailey, S., 2001. *Correction of Sun Glint Contamination on the SeaWiFS Ocean and Atmosphere Products*. Appl. Opt. 2001, 40, pp. 4790-4798.